NANO LETTERS

pubs.acs.org/NanoLett Letter

Ultranarrow TaS_2 Nanoribbons

Jeffrey D. Cain,[†] Sehoon Oh,[†] Amin Azizi,[†] Scott Stonemeyer, Mehmet Dogan, Markus Thiel, Peter Ercius, Marvin L. Cohen, and Alex Zettl*

Cite This: *Nano Lett.* 2021, 21, 3211−3217 Read Online

ACCESS | Metrics & More | Article Recommendations | Supporting Information

ABSTRACT: Imposing additional confinement in two-dimensional (2D) materials yields further control over their electronic, optical, and topological properties. However, synthesis of ultranarrow nanoribbons (NRs) remains challenging, particularly for transition metal dichalcogenides (TMDs), and synthesizing TMD NRs narrower than 50 nm has remained elusive. Here, we report the vapor-phase synthesis of ultranarrow TaS_2 NRs. The NRs are grown within carbon nanotubes, limiting their width and layer number, while stabilizing them against the environment. The NRs reach monolayer thickness and exhibit widths down to 2.5 nm. Atomic-resolution scanning transmission electron microscopy reveals the detailed atomic structure of the ultranarrow NRs and we observe a hitherto unseen atomic structure supermodulation of ordered defect arrays within the NRs. Density functional theory calculations show the presence of flat bands and boundary-localized states, and help identify the atomic configuration of the supermodulation. Nanotube-templated synthesis represents a unique, transferable, and broadly deployable route toward ultranarrow TMD NR growth.

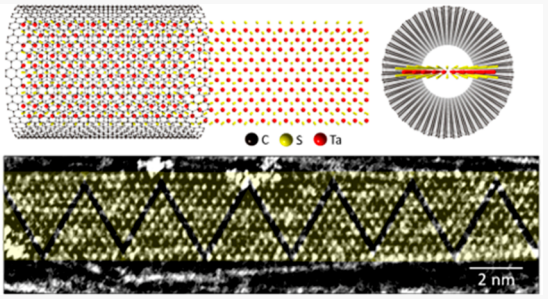

KEYWORDS: *Two-dimensional materials, nanoribbons, transition metal dichalcogenides, scanning transmission electron microscopy, flat bands, nanotubes*

In step with the resurgent interest in 2D materials, there have been extensive efforts toward engineering additional levels of confinement and, thus, lower dimensionality in few- and monolayer van der Waals bonded 2D structures. The greatest successes have been achieved in the fabrication and synthesis of graphene nanoribbons (GNRs), where rational bottom-up synthesis has been accomplished using the self-assembly of molecular precursors.[1,2] This has enabled the growth of GNRs with specific edge structures[3] and atomically precise widths,[4] as well as single GNR heterojunctions with engineered band alignment[5] and topology.[6] Exciting physics is similarly predicted to arise when 2D transition metal dichalcogenides (TMDs) are further constrained toward one-dimension (1D),[7] including the emergence of metal−insulator transitions,[8] enhanced thermoelectric performance,[9] ferromagnetism,[10,11] and tunable band gaps.[8]

However, the synthesis or fabrication of TMD NRs has lagged far behind that of GNRs both in terms of quality and width control. Past studies have relied upon top-down fabrication methods that require lithography and etching processes,[12,13] which results in NRs with widths greater than 50 nm—too large to observe quantum confinement effects—and with a high degree of structural disorder.[14] Molecular beam epitaxy has been used for the fabrication of ultranarrow $MoSe_2$ NRs,[15,16] but this method has little flexibility in implementation (e.g., substrate choice). Other bottom-up techniques, including chemical vapor deposition and vapor−liquid−solid growth, have recently been used to grow MoS_2 NRs,[17,18] resulting in ribbons with average widths >50 nm, again too large to access predicted quantum phenomena.

The templated growth of 1D nanomaterials using multi-walled carbon nanotubes (MWCNTs) has been successfully demonstrated for a variety of materials including elemental metals,[19] halides,[20] trichalcogenides,[21,22] and molecular chains,[23] where the synthesis generally results in nanowire- or chain-like structures. Nanoribbons have also been observed in nanotubes filled via solution based processes.[24,25] Here, we extend the method to ribbon-like morphologies, and demonstrate the growth of 2H-TaS_2 NRs with a simple vapor phase process. TaS_2 is a metallic TMD, which hosts multiple charge-density-wave (CDW) phases,[26−28] a Mott insulator state[29] and possible quantum spin liquid,[30] making it a unique material for the study of strongly correlated physics under extreme dimensional constraint.[31−33] We achieve TaS_2 NRs with thicknesses down to the monolayer limit (typical layer numbers are between 1 and 3), widths as low as 2.5 nm, and lengths greater than 100 nm. The MWCNT sheath fully encapsulates the TaS_2 NR, protecting it from interaction with

Received: February 3, 2021
Revised: March 29, 2021
Published: April 5, 2021

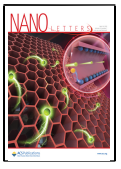

https://doi.org/10.1021/acs.nanolett.1c00481
Nano Lett. 2021, 21, 3211−3217

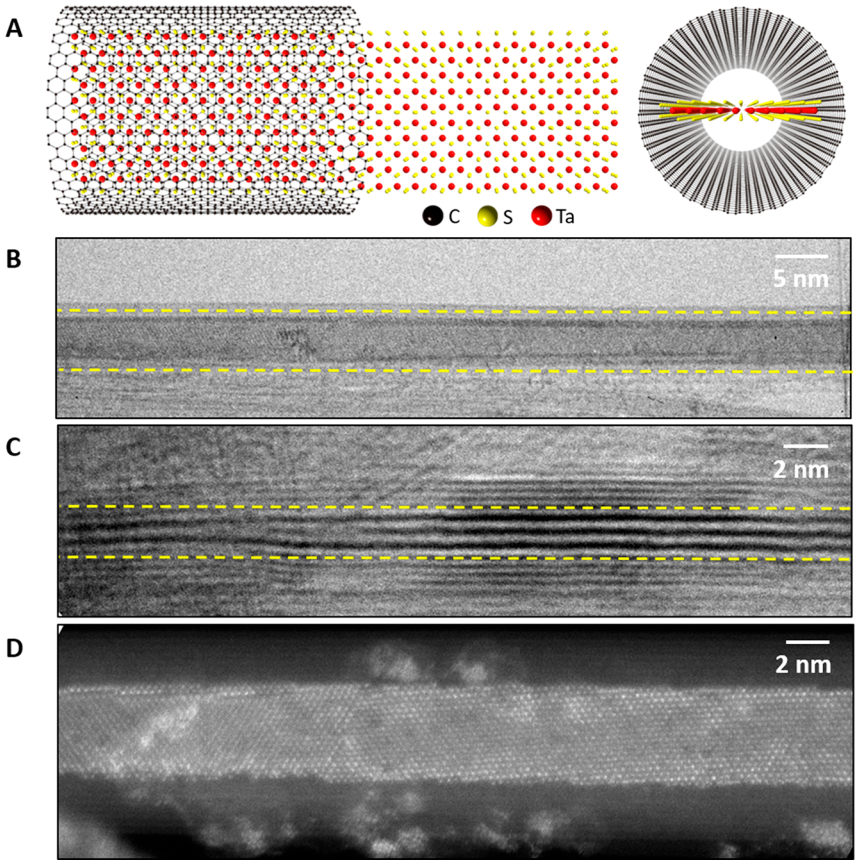

Figure 1. Imaging of ultranarrow TMD nanoribbons. (A) Schematic of TaS_2 nanoribbons templated by carbon nanotubes. (B) Plan view TEM image of 5 nm wide TaS_2 nanoribbon. (C) Side-view TEM image of a multilayer 2H-TaS_2 nanoribbon. (D) High-resolution ADF-STEM image of a TaS_2 nanoribbon with ∼4 nm width.

the environment. The growth produces NRs with controllable widths, clean NR surfaces and edges and enables easy handling (e.g., solution-based processing) and subsequent imaging of the structure and detailed atomic registry of NRs with transmission electron microscopy (TEM) and aberration-corrected annular dark-field scanning transmission electron microscopy (ADF-STEM). Furthermore, we observe and investigate previously unknown and unique periodic atomic superstructures defined by ordered defect arrays. First-principles calculations are used to elucidate the electronic structure of the NRs and atomic superstructure, revealing the presence of flat bands localized at the defect boundaries and edges.

TaS_2 NRs are grown within MWCNT using chemical vapor transport (CVT), described in detail in the Supporting Information. In brief, MWCNTs are first opened at the end via oxidation at high temperature;[34] the opened nanotubes are then coated onto the inner surface of a quartz ampule, which is filled with elemental Ta, S, and an iodine transport agent and sealed under vacuum. Synthesis is carried out in a gradient furnace in a manner similar to that used for single crystal TMD growth via CVT. We surmise that the growth mechanism is similar to the conventional vapor transport growth mechanism for MX_2 materials but subject to the additional geometrical constraint of the NT interior diameter.

Figure 1A shows a schematic of a monolayer TaS_2 NR within a carbon nanotube (for simplicity, a single-wall nanotube is shown), in both plan and end views. Figure 1B–D shows microscopy images of the as-synthesized material. Figure 1B shows a plan view TEM image of a 5 nm wide NR, while Figure 1C shows an edge view TEM image of a 3-layer NR. The dashed yellow lines in Figure 1B and 1C delineate the inner walls of the MWCNT. The strong contrast (dark lines are the TaS_2 atomic planes) in Figure 1C is because of the edge-on orientation, resulting in greater sample thickness; the measured interlayer distance (∼0.7 nm) matches well with that of bulk TaS_2 (0.7 nm).[35] Figure 1D is an ADF-STEM image (plan view) of a monolayer TaS_2 NR approximately 4 nm wide. The high crystallinity and uniform width of the NR is immediately apparent. It should be noted that Figure 1B and C (TEM) have the reverse contrast of Figure 1D (STEM).

We further explore the detailed atomic structure and phase of the TaS_2 NR using atomic-resolution ADF-STEM imaging. A NR with width 3.8 nm is presented in Figure 2A, where the hexagonal lattice characteristic of (monolayer) prismatically coordinated TaS_2 is clearly visible. A zoomed in portion of the ADF-STEM image of the NR in Figures 1D is also shown in 2B. Figure 2C is a simulated STEM image of a monolayer of TaS_2 with prismatic coordination. Figure 2D compares the line intensity profile along the dashed green box in the experimental image of Figure 2B and that of a simulated STEM image of monolayer TaS_2 (Figure 2C). This match suggests the experimental image is that of a monolayer TaS_2 NR with prismatic coordination, consistent with the bulk 2H phase, and further, is inconsistent with simulations performed on bilayer TaS_2. The presence of the prismatic phase is expected given the slow cool during synthesis, and the fact that the prismatic phase is the preferred phase at room temperature.

https://doi.org/10.1021/acs.nanolett.1c00481
Nano Lett. 2021, 21, 3211−3217

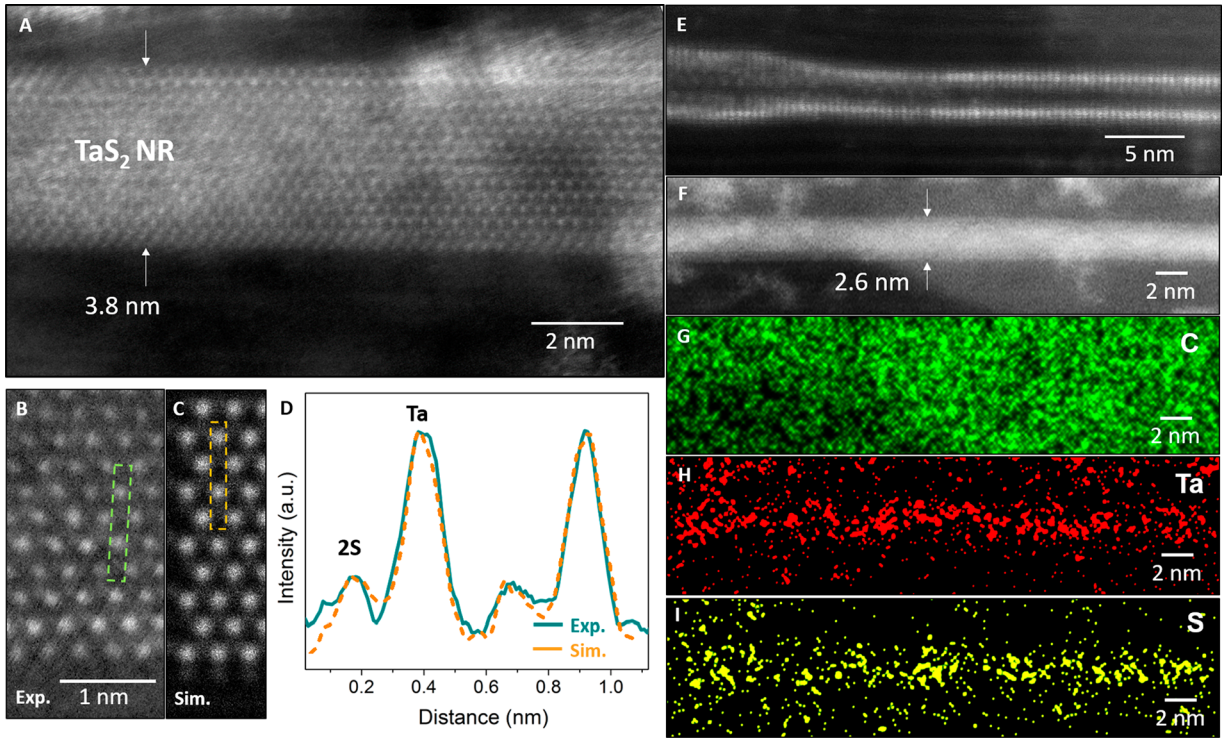

Figure 2. Atomic-resolution imaging of ultranarrow, monolayer TaS_2 nanoribbons. (A and B) Atomic resolution ADF-STEM images of TaS_2 nanoribbons. (C) STEM simulation of TaS_2 monolayer nanoribbon. (D) Line scan intensity profile comparison of the experimental (green) and simulated (orange) STEM images. (E) Side-view ADF-STEM image showing nanoribbon folding. (F−I) ADF-STEM reference image and EDS maps of C, Ta, and S, respectively.

The smallest NR width we have observed is 2.5 nm, and lengths of order 100 nm is not uncommon. The widest NR observed is 6 nm wide, and the average NR width is 3.8 nm. A histogram of NR widths is shown in Figure S1. In addition to strictly planar morphologies, some NRs also show curling at the edges (Figure 2E), presumably facilitated by the MWCNT confinement. The composition of the NRs is further supported by energy dispersive X-ray spectroscopy (EDS) (Figure 2G−I), which shows, over the width and length of the NR, a reasonably uniform distribution of Ta and S atoms. An ADF-STEM images of the mapped NR is shown for reference in Figure 2F. The (wider, as expected) carbon contribution is from the MWCNT. The EDS spectrum collected from the TaS_2 NR also clearly shows peaks of Ta and S (Figure S2); we also observe O (contamination), Si, and N (substrate), not shown in the displayed energy range. This further confirms the identity of the NR material.

We find that TaS_2 NRs can form not only with perfect atomic structure but also with striking periodic atomic superstructure, an example of which is presented in Figure 3. Figure 3A shows an atomic-resolution ADF-STEM image of a 3.3 nm wide TaS_2 NR containing an ordered, "zigzag"-like superstructure characterized by triangular domains of ideal TaS_2 lattice interrupted by boundaries of low STEM contrast. The zigzag structure is dramatically highlighted in a bandpass filtered version of the same image, presented in Figure 3B. The period of the perturbation is ∼9 unit cells.

Given the nature of bulk 2H-TaS_2, one may hypothesize that the periodic features arise from CDW-type distortions. As we discuss in more detail below, DFT calculations indicate that the TaS_2 NRs considered here appear to support CDWs, but the CDW amplitudes are small and CDWs are *not* the origin of the dramatic zigzag superstructure. Furthermore, the presence of CDW phases in the TaS_2 NR is not verified experimentally in this work. Rather, the superstructure arises from linear defect arrays. The atomic structure of the defect arrays is calculated via first-principles calculations (see below), and the relevant candidate structure is shown in Figure 3C. The structure is characterized by zigzag tracks of linearly formed S vacancies. A STEM simulation of this structure is shown in Figure 3D (STEM simulation details can be found in the Methods section of ref 36) for comparison with the experimental image in Figure 3E. Intensity line profiles across the boundary (along the dashed green box) in both the simulated (Figure 3F) and experimental images (Figure 3G) match, showing a Ta−Ta distance of ∼0.47 nm at the boundary versus ∼0.32 nm within the ideal TaS_2 lattice.

We expand on the discussion of our first-principles calculations based on DFT regarding the TaS_2 NRs. We investigate the atomic and electronic structures of TaS_2 bulk and ML, and the obtained atomic and electronic structures of the (prismatically coordinated) 2H-bulk and ML configurations (Figure S3) are consistent with other studies.[37,38] We investigate the atomic and electronic structure of NRs with various widths. First, we start with the NRs without structural defects (i.e., no vacancies, substitutions, or adatoms). The atomic positions of all the constructed structures are relaxed by minimizing the total energy. The obtained atomic and electronic structures of a NR (W = 2.99 nm) are shown in Figure 4A−C. Because of the metallicity and 1D nature, CDW-type distortions and corresponding partial gap openings are predicted in all the structures with various widths, but as noted previously, they do not match and are not the origin of the observed superstructure. We exclude the possibility that the

https://doi.org/10.1021/acs.nanolett.1c00481
Nano Lett. 2021, 21, 3211−3217

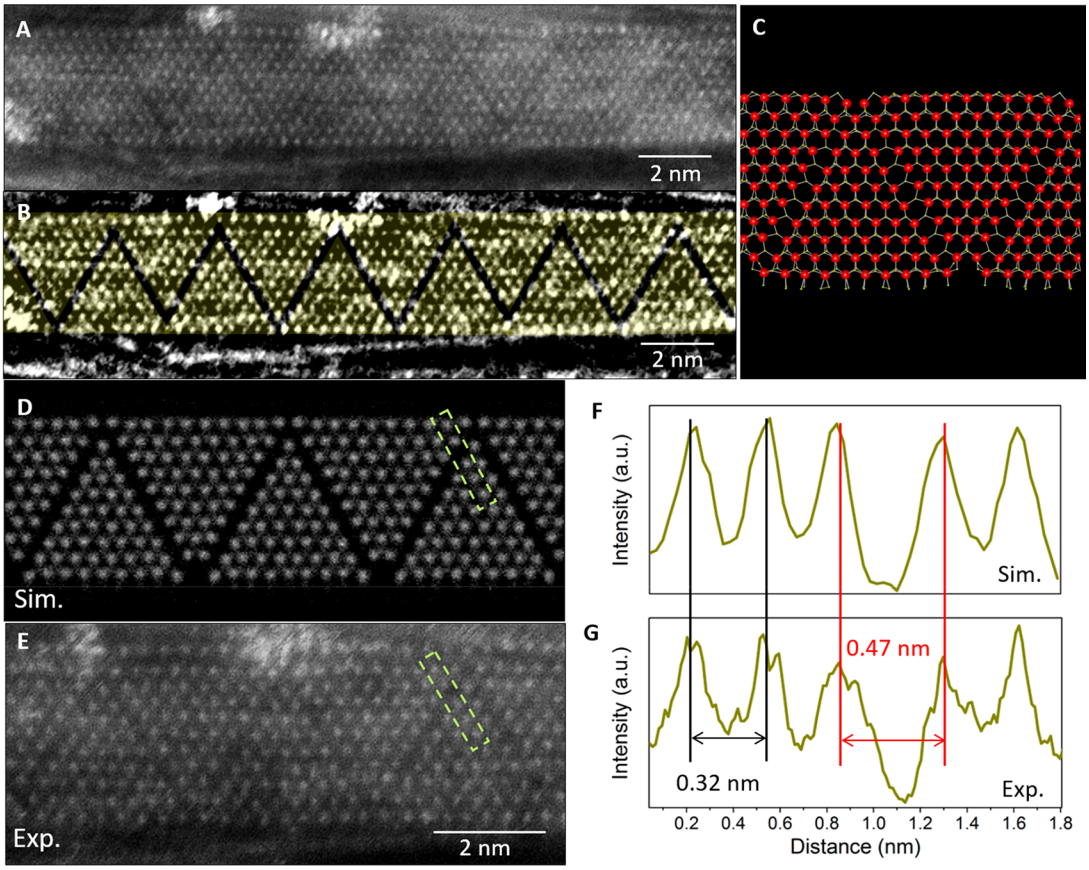

Figure 3. Periodic superstructure in TaS_2 nanoribbons. (A) ADF-STEM image and (B) its filtered version showing presence of zigzag-like atomic superstructure. The superstructure is identified as defect line arrays, with lines of missing S atoms. (C) Calculated atomic structure of defect line arrays in monolayer TaS_2 nanoribbons. (D) Simulated and (E) experimental STEM images of defect line arrays. Line intensity scans of (F) the simulated and (G) experimental images across the defect boundary along the dashed green boxes.

zigzag structure originates from CDW-type distortions and do not investigate the CDW phase any further, experimentally or theoretically. Figure 4A incorporates the predicted CDW distortions, but the amplitude of the distortions is too small to be readily apparent in the model, and furthermore, the CDW distortions are not commensurate with the experimentally observed zigzag pattern.

We next construct and optimize numerous candidate structures of the NRs with various types of structural defects for the zigzag boundaries. The atomic positions of all the constructed candidate structures are relaxed again by minimizing the total energy. Among the various candidate structures, we find a defect structure of NRs with various widths that is energetically favored compared to other candidate structures and matches well with the experimental STEM data. After careful analysis of the energetics of all the obtained structures (described below) and comparison with the STEM data, we conclude that the zigzag boundaries are linearly formed S vacancies in the NRs. As described above, Figure 3 shows the obtained atomic structures of a TaS_2 NR with W = 3.34 nm, the experimental STEM data, and the STEM simulation using the structures obtained by DFT for comparison, which agree well with each other. Figure 4D−H show the atomic and electronic structures of a NR with the zigzag defect array (W = 3.08 nm) in vacuum. In Figure 4D, the atomic structure is presented with the zigzag defect array denoted by L_1 and L_2, and the mirror planes denoted by M_1 and M_2. Figure 4E and F show the band structure unfolded with respect to the unit-cell of the primitive ML and the projected density of states (PDOS), respectively. A partial gap opening around the K-point is observed as shown in Figure 4E and there are two flat bands near the Fermi energy, E_F, (0.020 and 0.007 eV below E_F), denoted as ψ_1 and ψ_2, respectively, in Figure 4E and F. The real-space wave function of the flat bands reveals that they are localized edge states as shown in Figure 4G and H. The state ψ_1 is localized at the lower edge and has odd parity with respect to the mirror symmetries M_1 and M_2, while ψ_2 is at the upper edge and has even parity with respect to the mirror symmetries as shown in Figure 4G and H. A similar analysis is also performed on defect free and defective NRs of width 3.29 nm, the results of which are shown in Figure S4.

To analyze the stability of the NRs with various numbers of atoms in the unit-cell, we calculate the Gibbs free energy of formation, δG, of the obtained structures, which is defined as $\delta G = E_{NR} + n_{Ta}\mu_{Ta} + n_S\mu_S$, where E_{NR} is the total energy per atom of the NR, n_{Ta}, and n_S are the mole fractions of Ta and S atoms, respectively, and μ_{Ta} and μ_S are the chemical potentials of Ta and S, respectively. We choose μ_{Ta} and μ_S as the binding energies per atom of the α-Ta bulk and crown-shaped S_8 molecule, respectively. We find an interesting tendency that the structures with more S vacancies become more stable. For a quantitative analysis, we measure the ratio R of the number of Ta atoms to that of S atoms, which is defined as $R = n_S/n_{Ta}$. The NRs without structural defects have R = 2.14−2.20 > R_{bulk} = 2.0, because the edges are S-terminated, and the confined

https://doi.org/10.1021/acs.nanolett.1c00481
Nano Lett. 2021, 21, 3211−3217

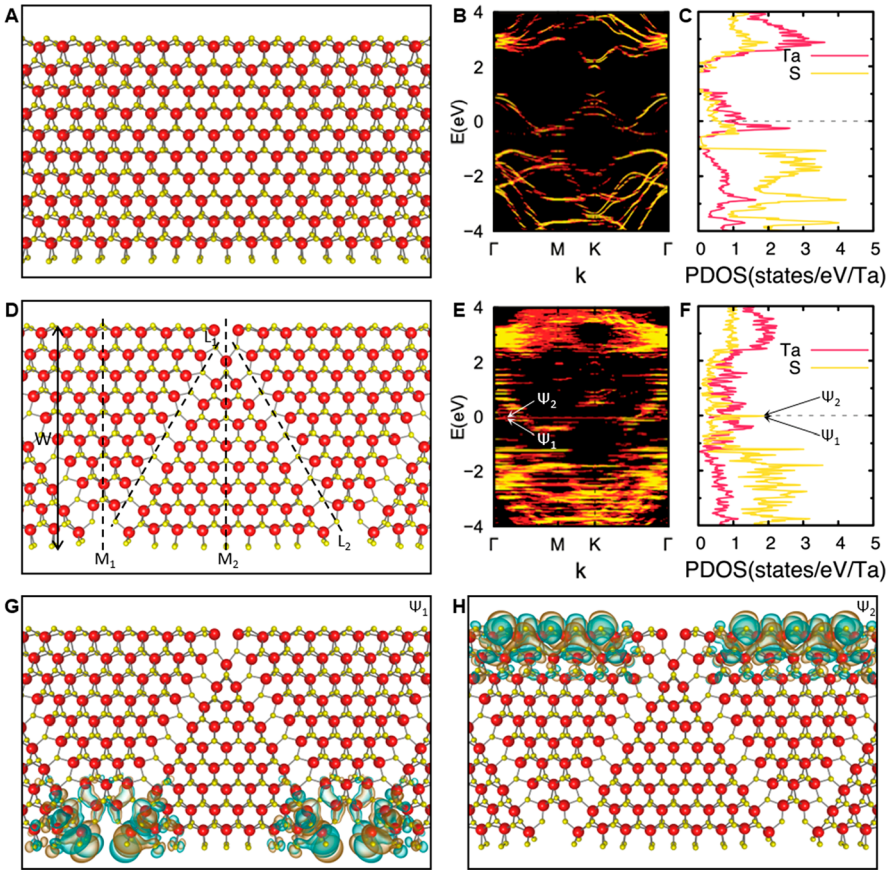

Figure 4. Atomic and electronic structure of TaS_2 NRs with and without defect line arrays. (A−C) Atomic and electronic structures of the NR of W = 2.99 nm without the zigzag defect are shown. The structure does have CDW distortions, but the distortion amplitude is too small to be seen by eye in panel A. Panel A shows the atomic structure in planar view; panel B shows the electronic band structure; and panel C shows the PDOS of the NR. (D−H) Atomic and electronic structures of NR of W = 3.08 nm with zigzag defect array are shown. (D) Atomic structure of the NR is shown in the planar view, where the zigzag boundaries of S vacancies are represented by black dashed lines denoted as L_1 and L_2, and the mirror planes are represented by vertical black dashed lines denoted as M_1 and M_2. (E) Electronic band structure and (F) the PDOS of the NR. The localized edge states are marked by arrows and denoted as ψ_1 and ψ_2. (G, H) Real-space wave functions of the localized edges states ψ_1 and ψ_2. The isosurfaces for the positive and negative values of the real-space wave functions are shaded in cyan and orange, respectively. In the atomic structures, Ta and S atoms are represented by red and yellow spheres, respectively. The bands in panels B and E are unfolded with respect to the unit-cell of the primitive ML. The density of states projected to Ta and S atoms are represented by red and yellow lines, respectively. The Fermi energy is set to zero.

nature of the NR. The presence of S vacancies reduces R, and the stable calculated structures agreeing well with the experimental data have R = 2.00−2.01 (Table 1). We note that other kinds of defect ordering, such as Ta adatoms, can also reduce R and thereby enhance structural stability. We speculate that stabilization of the structure afforded by driving $R \rightarrow 2$ is the main driving force of the formation of the zigzag defects with S vacancies.

It is worth emphasizing the following: First, the encapsulation of the NRs in CNTs does not alter the electronic structures of the NRs significantly except for the slight changes of E_F because of the charge transfer between NRs and CNTs. The calculated charge transfer q from CNTs to NRs is ∼0.02 e per Ta atom, where e is the electron charge. Second, the interaction between the CNT's inner wall and the NR's edges is mainly van der Waals interaction. No appreciable amount of covalent bonding is found between the NRs and the CNTs in the DFT calculations. Third, no significant magnetic moment is found in all of the fully magnetic calculations with spin−orbit interaction. Last, the presence of the time-reversal symmetry and mirror symmetry in the prismatic phase

Table 1. Structural and Energetic Properties of TaS_2NRs[a]

	NR-1	NR-2
phase	prismatic	prismatic
boundary shape	zigzag	zigzag
defects	S vacancies	S vacancies
symmetry	mirror	mirror
W (nm)	3.08	3.34
N_{Ta}	99	120
N_S	198	240
R	2.00	2.00
δG (eV)	−0.573	−0.633

[a]The structure phase, boundary shape, type of defects, symmetry, and the width, W, of two TaS_2 NRs obtained with DFT calculations. The number of Ta (S) atoms in the unit cell, N_{Ta} (N_S), and the ratio of N_{Ta} to N_S atoms, R. The Gibbs free energy of formation, δG, is defined as $E_{NR} + n_{Ta}\mu_{Ta} + n_S\mu_S$, where E_{NR} is the total energy per atom of the NR, n_{Ta}, and n_S are the mole fractions of Ta and S atoms, respectively, and μ_{Ta} and μ_S are the binding energies per atom of the α-Ta bulk and crown-shaped S_8 molecule, respectively.

https://doi.org/10.1021/acs.nanolett.1c00481
Nano Lett. 2021, 21, 3211−3217

indicates the potential for interesting topological properties in these NRs.

In summary, we have demonstrated a method that enables the synthesis of ultranarrow TMD NRs via a simple and broadly deployable gas phase process, using MWCNTs to template their growth. Our method results in TaS_2 NRs with widths below 3 nm, and lengths greater than 100 nm, while reaching the ML limit. Further, the nanoconfined growth of the NRs results in the formation of ordered arrays of linear defects in the TaS_2 lattice. DFT calculations reveal the characteristics of the defect arrays with spatial symmetries and electronic structures with localized edge and boundary states. The reported nanotube templated growth represents a versatile platform for the synthesis of ultranarrow TMD NRs and the exploration of the materials under constraint in multiple dimensions.

■ ASSOCIATED CONTENT

Supporting Information

The Supporting Information is available free of charge at https://pubs.acs.org/doi/10.1021/acs.nanolett.1c00481.

Materials and methods, supplementary text, and Figures S1−S4 (PDF)

■ AUTHOR INFORMATION

Corresponding Author

Alex Zettl − *Department of Physics, University of California at Berkeley, Berkeley, California 94720, United States; Materials Sciences Division, Lawrence Berkeley National Laboratory, Berkeley, California 94720, United States; Kavli Energy NanoSciences Institute at the University of California at Berkeley and the Lawrence Berkeley National Laboratory, Berkeley, California 94720, United States*; Email: azettl@berkeley.edu

Authors

Jeffrey D. Cain − *Department of Physics, University of California at Berkeley, Berkeley, California 94720, United States; Materials Sciences Division, Lawrence Berkeley National Laboratory, Berkeley, California 94720, United States; Kavli Energy NanoSciences Institute at the University of California at Berkeley and the Lawrence Berkeley National Laboratory, Berkeley, California 94720, United States;* orcid.org/0000-0001-9244-4271

Sehoon Oh − *Department of Physics, University of California at Berkeley, Berkeley, California 94720, United States; Materials Sciences Division, Lawrence Berkeley National Laboratory, Berkeley, California 94720, United States;* orcid.org/0000-0003-0518-4091

Amin Azizi − *Department of Physics, University of California at Berkeley, Berkeley, California 94720, United States; Kavli Energy NanoSciences Institute at the University of California at Berkeley and the Lawrence Berkeley National Laboratory, Berkeley, California 94720, United States;* orcid.org/0000-0001-9955-7228

Scott Stonemeyer − *Department of Physics and Department of Chemistry, University of California at Berkeley, Berkeley, California 94720, United States; Materials Sciences Division, Lawrence Berkeley National Laboratory, Berkeley, California 94720, United States; Kavli Energy NanoSciences Institute at the University of California at Berkeley and the Lawrence Berkeley National Laboratory, Berkeley, California 94720, United States;* orcid.org/0000-0002-8135-5625

Mehmet Dogan − *Department of Physics, University of California at Berkeley, Berkeley, California 94720, United States; Materials Sciences Division, Lawrence Berkeley National Laboratory, Berkeley, California 94720, United States*

Markus Thiel − *Department of Physics, University of California at Berkeley, Berkeley, California 94720, United States*

Peter Ercius − *The Molecular Foundry, Lawrence Berkeley National Laboratory, Berkeley, California 94720, United States;* orcid.org/0000-0002-6762-9976

Marvin L. Cohen − *Department of Physics, University of California at Berkeley, Berkeley, California 94720, United States; Materials Sciences Division, Lawrence Berkeley National Laboratory, Berkeley, California 94720, United States*

Complete contact information is available at: https://pubs.acs.org/10.1021/acs.nanolett.1c00481

Author Contributions

†J.D.C., S.O., and A.A. contributed equally. J.D.C. and A.Z. conceived the idea; J.D.C. and M.T. synthesized the materials; J.D.C., A.A., S.S., and P.E. performed electron microscopy data acquisition and analysis. S.O. and M.D. carried out density functional calculations. S.O. and M.D. did the theoretical analysis. A.Z. and M.L.C supervised the project; J.D.C, A.A., and S.O. wrote the manuscript with input from all authors.

Notes

The authors declare no competing financial interest.

■ ACKNOWLEDGMENTS

This work was primarily funded by the U.S. Department of Energy, Office of Science, Office of Basic Energy Sciences, Materials Sciences and Engineering Division, under Contract No. DE-AC02-05-CH11231 within the sp^2-Bonded Materials Program (KC2207) and the Nanomachines Program which provided for synthesis of the chains, TEM structural characterization, and theoretical modeling of relaxed structure of the NRs. The elemental mapping work was funded by the U.S. Department of Energy, Office of Science, Office of Basic Energy Sciences, Materials Sciences and Engineering Division, under Contract No. DE-AC02-05-CH11231 within the van der Waals Heterostructures Program (KCWF16). Work at the Molecular Foundry (TEAM 0.5 characterization) was supported by the Office of Science, Office of Basic Energy Sciences, of the U.S. Department of Energy under Contract No. DE-AC02-05-CH11231. Support was also provided by the National Science Foundation under Grant No. DMR-1807233, which provided for preparation of opened nanotubes, and Grant No. DMR 1926004, which provided for theoretical calculations of the electronic band structure of the materials. Computational resources were provided by the DOE at Lawrence Berkeley National Laboratory's NERSC facility and the NSF through XSEDE resources at NICS.

■ REFERENCES

(1) Bennett, P. B.; Pedramrazi, Z.; Madani, A.; Chen, Y.-C.; de Oteyza, D. G.; Chen, C.; Fischer, F. R.; Crommie, M. F.; Bokor, J. Bottom-up Graphene Nanoribbon Field-Effect Transistors. *Appl. Phys. Lett.* **2013**, *103* (25), 253114.

(2) Chen, Y.-C.; de Oteyza, D. G.; Pedramrazi, Z.; Chen, C.; Fischer, F. R.; Crommie, M. F. Tuning the Band Gap of Graphene Nanoribbons Synthesized from Molecular Precursors. *ACS Nano* **2013**, *7*, 6123.
(3) Tao, C.; Jiao, L.; Yazyev, O. V.; Chen, Y.-C.; Feng, J.; Zhang, X.; Capaz, R. B.; Tour, J. M.; Zettl, A.; Louie, S. G.; et al. Spatially Resolving Edge States of Chiral Graphene Nanoribbons. *Nat. Phys.* **2011**, *7* (8), 616−620.
(4) Cai, J.; Pignedoli, C. A.; Talirz, L.; Ruffieux, P.; Söde, H.; Liang, L.; Meunier, V.; Berger, R.; Li, R.; Feng, X.; et al. Graphene Nanoribbon Heterojunctions. *Nat. Nanotechnol.* **2014**, *9* (11), 896−900.
(5) Rizzo, D. J.; Veber, G.; Cao, T.; Bronner, C.; Chen, T.; Zhao, F.; Rodriguez, H.; Louie, S. G.; Crommie, M. F.; Fischer, F. R. Topological Band Engineering of Graphene Nanoribbons. *Nature* **2018**, *560* (7717), 204−208.
(6) Nguyen, G. D.; Tsai, H. Z.; Omrani, A. A.; Marangoni, T.; Wu, M.; Rizzo, D. J.; Rodgers, G. F.; Cloke, R. R.; Durr, R. A.; Sakai, Y.; et al. Atomically Precise Graphene Nanoribbon Heterojunctions from a Single Molecular Precursor. *Nat. Nanotechnol.* **2017**, *12* (11), 1077−1082.
(7) Chowdhury, T.; Sadler, E. C.; Kempa, T. J. Progress and Prospects in Transition-Metal Dichalcogenide Research beyond 2D. *Chem. Rev.* **2020**, *120*, 12563−12591.
(8) Dolui, K.; Pemmaraju, C. D.; Sanvito, S. Electric Field Effects on Armchair MoS 2 Nanoribbons. *ACS Nano* **2012**, *6*, 4823−4834.
(9) Zhang, Z.; Xie, Y.; Peng, Q.; Chen, Y. A Theoretical Prediction of Super High-Performance Thermoelectric Materials Based on MoS2/WS2 Hybrid Nanoribbons. *Sci. Rep.* **2016**, *6* (1), 21639.
(10) Botello-Méndez, A. R.; López-Urías, F.; Terrones, M.; Terrones, H. Metallic and Ferromagnetic Edges in Molybdenum Disulfide Nanoribbons. *Nanotechnology* **2009**, *20* (32), 325703.
(11) Davelou, D.; Kopidakis, G.; Kaxiras, E.; Remediakis, I. N. Nanoribbon Edges of Transition-Metal Dichalcogenides: Stability and Electronic Properties. *Phys. Rev. B: Condens. Matter Mater. Phys.* **2017**, *96* (16), 165436.
(12) Li, Q.; Newberg, J. T.; Walter, E. C.; Hemminger, J. C.; Penner, R. M. Polycrystalline Molybdenum Disulfide (2H-MoS_2) Nano-and Microribbons by Electrochemical/Chemical Synthesis. *Nano Lett.* **2004**, *4*, 277−281.
(13) Pak, Y.; Kim, Y.; Lim, N.; Min, J.-W.; Park, W.; Kim, W.; Jeong, Y.; Kim, H.; Kim, K.; Mitra, S.; et al. Scalable Integration of Periodically Aligned 2D-MoS_2 Nanoribbon Array. *APL Mater.* **2018**, *6* (7), 076102.
(14) Li, Y.; Moy, E. C.; Murthy, A. A.; Hao, S.; Cain, J. D.; Hanson, E. D.; DiStefano, J. G.; Chae, W. H.; Li, Q.; Wolverton, C.; et al. Large-Scale Fabrication of MoS_2 Ribbons and Their Light-Induced Electronic/Thermal Properties: Dichotomies in the Structural and Defect Engineering. *Adv. Funct. Mater.* **2018**, *28* (13), 1704863.
(15) Cheng, F.; Xu, H.; Xu, W.; Zhou, P.; Martin, J.; Loh, K. P. Controlled Growth of 1D $MoSe_2$ Nanoribbons with Spatially Modulated Edge States. *Nano Lett.* **2017**, *17*, 1116−1120.
(16) Poh, S. M.; Tan, S. J. R.; Zhao, X.; Chen, Z.; Abdelwahab, I.; Fu, D.; Xu, H.; Bao, Y.; Zhou, W.; Loh, K. P. Large Area Synthesis of 1D-$MoSe_2$ Using Molecular Beam Epitaxy. *Adv. Mater.* **2017**, *29* (12), 1605641.
(17) Li, S.; Lin, Y.-C.; Zhao, W.; Wu, J.; Wang, Z.; Hu, Z.; Shen, Y.; Tang, D.-M.; Wang, J.; Zhang, Q.; et al. Vapour-Liquid-Solid Growth of Monolayer MoS 2 Nanoribbons. *Nat. Mater.* **2018**, *17*, 535−542.
(18) Chowdhury, T.; Kim, J.; Sadler, E. C.; Li, C.; Lee, S. W.; Jo, K.; Xu, W.; Gracias, D. H.; Drichko, N. V.; Jariwala, D.; et al. Substrate-Directed Synthesis of MoS2 Nanocrystals with Tunable Dimensionality and Optical Properties. *Nat. Nanotechnol.* **2020**, *15* (1), 29−34.
(19) Pham, T.; Fathalizadeh, A.; Shevitski, B.; Turner, S.; Aloni, S.; Zettl, A. A Universal Wet-Chemistry Route to Metal Filling of Boron Nitride Nanotubes. *Nano Lett.* **2016**, *16* (1), 320−325.
(20) Philp, E.; Sloan, J.; Kirkland, A. I.; Meyer, R. R.; Friedrichs, S.; Hutchison, J. L.; Green, M. L. H. An Encapsulated Helical One-Dimensional Cobalt Iodide Nanostructure. *Nat. Mater.* **2003**, *2* (12), 788−791.
(21) Pham, T.; Oh, S.; Stetz, P.; Onishi, S.; Kisielowski, C.; Cohen, M. L.; Zettl, A. Torsional Instability in the Single-Chain Limit of a Transition Metal Trichalcogenide. *Science (Washington, DC, U. S.)* **2018**, *361* (6399), 263−266.
(22) Meyer, S.; Pham, T.; Oh, S.; Ercius, P.; Kisielowski, C.; Cohen, M. L.; Zettl, A. Metal-Insulator Transition in Quasi-One-Dimensional HfTe3 in the Few-Chain Limit. *Phys. Rev. B: Condens. Matter Mater. Phys.* **2019**, *100*, No. 041403(R).
(23) Pham, T.; Oh, S.; Stonemeyer, S.; Shevitski, B.; Cain, J. D.; Song, C.; Ercius, P.; Cohen, M. L.; Zettl, A. Emergence of Topologically Nontrivial Spin-Polarized States in a Segmented Linear Chain. *Phys. Rev. Lett.* **2020**, *124* (20), 206403.
(24) Wang, Z.; Zhao, K.; Li, H.; Liu, Z.; Shi, Z.; Lu, J.; Suenaga, K.; Joung, S.-K.; Okazaki, T.; Jin, Z.; et al. Ultra-Narrow WS_2 Nanoribbons Encapsulated in Carbon Nanotubes. *J. Mater. Chem.* **2011**, *21*, 171−180.
(25) Wang, Z.; Li, H.; Liu, Z.; Shi, Z.; Lu, J.; Suenaga, K.; Joung, S.-K.; Okazaki, T.; Gu, Z.; Zhou, J.; et al. Mixed Low-Dimensional Nanomaterial: 2D Ultranarrow MoS_2 Inorganic Nanoribbons Encapsulated in Quasi-1D Carbon Nanotubes. *J. Am. Chem. Soc.* **2010**, *132* (39), 13840−13847.
(26) Tsen, A. W.; Hovden, R.; Wang, D.; Kim, Y. D.; Okamoto, J.; Spoth, K. A.; Liu, Y.; Lu, W.; Sun, Y.; Hone, J. C.; et al. Structure and Control of Charge Density Waves in Two-Dimensional 1T-TaS2. *Proc. Natl. Acad. Sci. U. S. A.* **2015**, *112* (49), 15054−15059.
(27) Burk, B.; Thomson, R. E.; Clarke, J.; Zettl, A. Surface and Bulk Charge Density Wave Structure in 1 T-TaS2. *Science* **1992**, *257* (5068), 362−364.
(28) Wilson, J. A.; Di Salvo, F. J.; Mahajan, S. Charge-Density Waves and Superlattices in the Metallic Layered Transition Metal Dichalcogenides. *Adv. Phys.* **1975**, *24* (2), 117−201.
(29) Sipos, B.; Kusmartseva, A. F.; Akrap, A.; Berger, H.; Forró, L.; Tutiš, E. From Mott State to Superconductivity in 1T-TaS_2. *Nat. Mater.* **2008**, *7*, 960−965.
(30) Law, K. T.; Lee, P. A. 1T-TaS2 as a Quantum Spin Liquid. *Proc. Natl. Acad. Sci. U. S. A.* **2017**, *114* (27), 6996−7000.
(31) Burk, B.; Thomson, R. E.; Zettl, A.; Clarke, J. Charge-Density-Wave Domains in 1T-TaS_2 Observed by Satellite Structure in Scanning-Tunneling-Microscopy Images. *Phys. Rev. Lett.* **1991**, *66*, 3040.
(32) Thomson, R. E.; Burk, B.; Zettl, A.; Clarke, J. Scanning Tunneling Microscopy of the Charge-Density-Wave Structure in 1T-TaS_2. *Phys. Rev. B: Condens. Matter Mater. Phys.* **1994**, *49*, 16899.
(33) Yang, Y.; Fang, S.; Fatemi, V.; Ruhman, J.; Navarro-Moratalla, E.; Watanabe, K.; Taniguchi, T.; Kaxiras, E.; Jarillo-Herrero, P. Enhanced Superconductivity upon Weakening of Charge Density Wave Transport in 2H-TaS_2 in the Two-Dimensional Limit. *Phys. Rev. B: Condens. Matter Mater. Phys.* **2018**, *98* (3), 035203.
(34) Ajayan, P. M.; Ebbesen, T. W.; Ichihashi, T.; Iijima, S.; Tanigaki, K.; Hiura, H. Opening Carbon Nanotubes with Oxygen and Implications for Filling. *Nature* **1993**, *362* (6420), 522−525.
(35) Hovden, R.; Tsen, A. W.; Liu, P.; Savitzky, B. H.; El Baggari, I.; Liu, Y.; Lu, W.; Sun, Y.; Kim, P.; Pasupathy, A. N.; et al. Atomic Lattice Disorder in Charge-Density-Wave Phases of Exfoliated Dichalcogenides (1T-TaS_2). *Proc. Natl. Acad. Sci. U. S. A.* **2016**, *113* (41), 11420−11424.
(36) Ophus, C. A Fast Image Simulation Algorithm for Scanning Transmission Electron Microscopy. *Adv. Struct. Chem. Imaging* **2017**, *3* (1), 13.
(37) Lazar, P.; Martincová, J.; Otyepka, M. Structure, Dynamical Stability, and Electronic Properties of Phases in TaS_2 from a High-Level Quantum Mechanical Calculation. *Phys. Rev. B: Condens. Matter Mater. Phys.* **2015**, *92* (22), 224104.
(38) Sanders, C. E.; Dendzik, M.; Ngankeu, A. S.; Eich, A.; Bruix, A.; Bianchi, M.; Miwa, J. A.; Hammer, B.; Khajetoorians, A. A.; Hofmann, P. Crystalline and Electronic Structure of Single-Layer TaS_2. *Phys. Rev. B: Condens. Matter Mater. Phys.* **2016**, *94* (8), 081404.

https://doi.org/10.1021/acs.nanolett.1c00481
Nano Lett. 2021, 21, 3211−3217